On non-monotonic variation of hydrodynamically focused width in a rectangular microchannel

Siddhartha Tripathi, Pritish Chakravarty and Amit Agrawal*

Department of Mechanical Engineering, Indian Institute of Technology Bombay, Powai, Mumbai 400 076, India

This article presents a comprehensive theoretical model and limited experimental results for describing two-dimensional hydrodynamic focusing in microchannels involving immiscible fluids. It is shown that the normalized focused sample width depends on three non-dimensional parameters – the flow rate ratio, viscosity ratio and aspect ratio. A theory encompassing the effects of all these parameters is developed. Whereas the effects of flow rate ratio and viscosity ratio on the focused sample width are monotonic in nature, those of aspect ratio can be non-monotonic. We report existence of a viscosity ratio beyond which the normalized width decreases with an increase in the aspect ratio, and for viscosity ratio less than a critical value the normalized width increases with increase in the aspect ratio. This parameter range where the minimum sample width is obtained is further analysed. The effect of aspect ratio and flow rate ratio have been validated experimentally using oil and water based systems. A physical explanation of the variation of sample width with aspect ratio along with microchannel-design guidelines are also provided in this study. We demonstrate that the derived results are more general than the available theoretical models. This comprehensive theory can eventually be employed for predicting hydrodynamically focused width in microdevices and for employing optimal aspect ratio microchannels, without incurring the cost of experiments and human effort.

Keywords: Aspect ratio, focused width, flow rate ratio, microfluidics, oil–water experiments, viscosity ratio.

HYDRODYNAMIC flow focusing is an important phenomenon in the area of microfluidics with a wide range of applications. It can be described as the squeezing of a sample fluid using a sheath fluid. The amount of focusing depends on the flow conditions, fluid properties and geometry. Hydrodynamic focusing is a simple yet effective technique for flow focusing and control. It has been successfully utilized in conventional flow cytometers and microflow cytometers to enable analysis of individual cells/particles[1–6]. Hydrodynamic focusing has numerous other applications such as cell patterning[7,8], flow switching[9–11], DNA deformation[12], micromixers[13–15], droplet generators[16], measuring ATP from RBCs[17], in micro-PIV as a seeding technique[18,19], and for microfabrication and patterning inside a capillary[20]. The major advantage of hydrodynamic focusing is that it avoids damage to biological cells and reduces the volume of sample necessary for continuous flow experiments.

Being able to predict the focused sample width is a crucial aspect of hydrodynamic focusing. Thus, the formulation of a comprehensive theoretical model for predicting the focused sample width is of paramount importance; various research groups have formulated expressions for the focused sample width. Knight *et al.*[13] showed that the focused sample width does not depend on the magnitude of the applied pressure, rather on the ratio of the pressure applied to the side and inlet streams. Stiles *et al.*[21] proposed a design in which a single syringe pump was used and the flow rates were controlled by the resistance of the channels. The focused sample width was expressed in terms of the flow rate ratios only; the viscosities of the two fluids was however assumed to be equal. Their formula was used towards the development of a micro-Coulter counter[22]. The effect of different viscosity of fluids on hydrodynamic focusing has been considered in refs 23–25.

Stiles and Fletcher[23] studied the viscous spreading of two immiscible liquids flowing side by side in a rectangular microchannel. They derived a formula relating viscous spreading to the aspect ratio of microchannels, flow rate ratio and viscosity ratio of fluids, however, their study was not extended to the case of hydrodynamic focusing nor was it validated experimentally. Wu and Nguyen[24] studied hydrodynamic focusing with diffusive dispersion and established the influence of viscosity ratio and flow ratio on focused width of the sample. Their study however did not consider the effects of aspect ratio; a final formula for calculating the focused sample width was also not given. Lee *et al.*[11] worked towards providing a generalized model for flow focusing which imposed no restriction on the aspect ratio of the channel. Their model predicts both the location and width of the focused stream, and their results indicated that the focused width decreases as the flow ratio increases; for a given flow ratio, the focused width decreases monotonically with an

*For correspondence. (e-mail: amit.agrawal@iitb.ac.in)

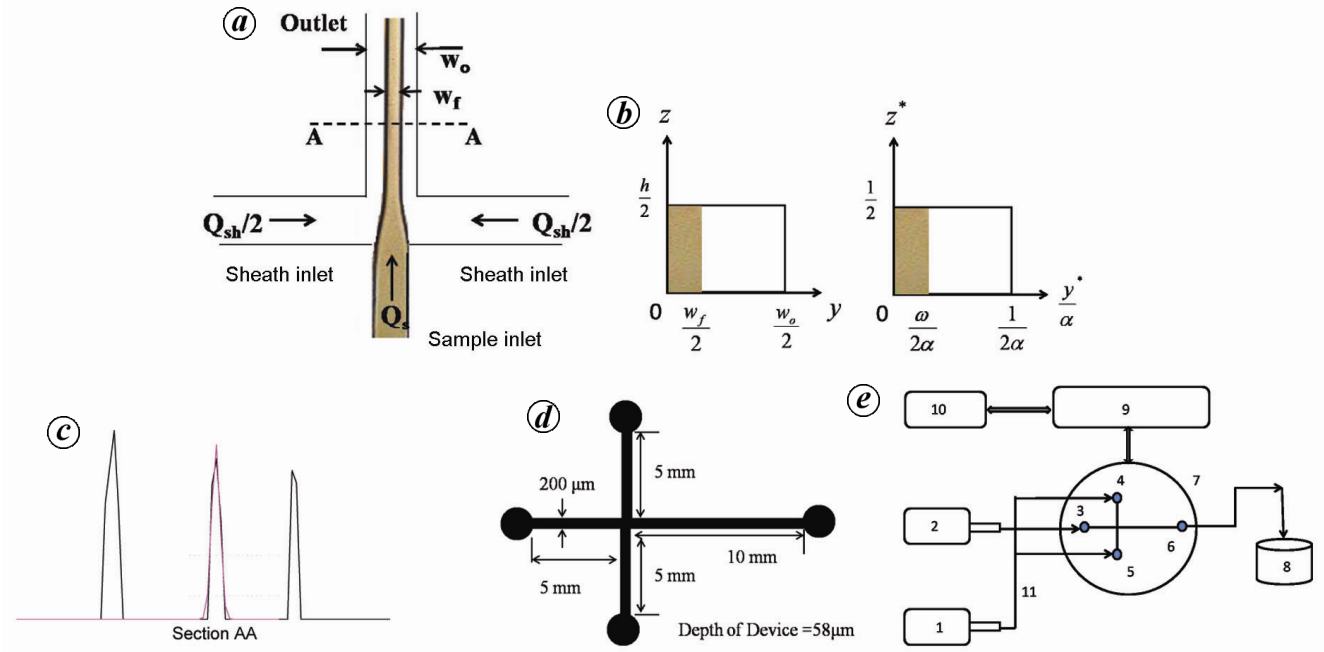

Figure 1. ***a***, A touched-up image with dye providing a schematic of hydrodynamic focusing in a cross-shaped microchannel. ***b***, Cross-section of the microchannel employed for the theoretical development. ***c***, Intensity plot along width of the microchannel cross-section. ***d***, Geometrical details of the cross-shaped channel employed in the experiments. ***e***, Schematic of the experimental setup (1, 2, Syringe pumps; 3, Inlet of sample; 4, 5, Inlet of sheath; 6, Outlet; 7, Microfluidic device; 8, Outlet reservoir; 9, Microscope with attached CCD; 10, Computer; 11, Microflex tubing).

increase in the aspect ratio. However, the analysis does not consider that the sheath and sample fluids can have different viscosities. We show that for non-unity viscosity ratio cases, the focused width can display a non-monotonic variation with aspect ratio. In a separate study, it was found by Olsen *et al.*[26] that the focused width is also dependent on the geometry of the microfluidic channels. They showed that the angle between the side channels and the main channel affects the focused width; as this angle approaches 90°, the focused width becomes narrower. It is therefore observed that there is a lack of a final holistic expression to calculate the focused sample width.

The focused width of the sample is a function of the three governing parameters: the flow ratio, F (sheath/sample), aspect ratio, α (height/width) of the microchannel and viscosity ratio, β (sample/sheath) of the fluids (see Appendix A). The aspect ratio depends on the microchannel employed while the viscosity ratio depends on the fluids; their values are expected to be different between two sets of experiments. Therefore, an analytical expression against which the experimental results can be compared will be particularly useful.

Theoretical development

This section discusses the relevant theory and solution of the equations. A discussion on the limiting cases and a comparison with other theoretical results in literature is also presented. It is shown that the obtained result is indeed more general as compared to the existing solutions.

Derivation of expression for focused sample width

The following theoretical model describes a flowing fluid (sample) sandwiched between two layers of another fluid (sheath) flowing in a microchannel having a rectangular cross-section. The direction of flow is along the x-direction, the width is along the y-direction and the height is along the z-direction (Figure 1 *a* and *b*). As seen from the figure, the model is symmetric with respect to the y and z-axes. Thus, only one quarter of the cross-sectional plane needs to be considered.

To arrive at a theoretical expression for determining the focused width of the sample fluid, we assume fluids to be Newtonian and immiscible, and flow to be incompressible, steady and laminar, fully developed with negligible interfacial tension at the interface. Note that the analysis applies to the straight portion of the focused stream, i.e., away from the junction. We first apply the Navier–Stokes equations to both the sample and sheath fluids

$$\frac{\partial^2 u_s}{\partial y^2} + \frac{\partial^2 u_s}{\partial z^2} = \frac{1}{\eta_s}\frac{\partial p}{\partial x} \tag{1}$$

$$\frac{\partial^2 u_{sh}}{\partial y^2}+\frac{\partial^2 u_{sh}}{\partial z^2}=\frac{1}{\eta_{sh}}\frac{\partial p}{\partial x}. \tag{2}$$

where u_s is sample fluid velocity, u_{sh} the sheath fluid velocity, η_s the viscosity of sample fluid, η_{sh} the viscosity of sheath fluid and p is the pressure.

Now, non-dimensionalizing the above equations using $u_s^* = u_s/u_0$; $u_{sh}^* = u_{sh}/u_0$; $y^* = y/w_0$; $z^* = z/h$; $x^* = x/L$, $\omega = w_f/w_0$, and P is given by eq. (14), leads to the following equations in non-dimensional form

$$\alpha^2\frac{\partial^2 u_s^*}{\partial y^{*2}}+\frac{\partial^2 u_s^*}{\partial z^{*2}}=P \tag{3}$$

$$\alpha^2\frac{\partial^2 u_{sh}^*}{\partial y^{*2}}+\frac{\partial^2 u_{sh}^*}{\partial z^{*2}}=P\beta. \tag{4}$$

where u_s^* is normalized sample fluid velocity, u_{sh}^* the normalized sheath fluid velocity, u_0 the maximum sheath fluid velocity, y^* the normalized co-ordinate along width of the microchannel, z^* the normalized co-ordinate along height of the microchannel, x^* the normalized co-ordinate along length of microchannel, h the height of microchannel, L the length of exit arm of microchannel, w_f the hydrodynamically focused sample width, w_0 the width of microchannel and ω is the normalized focused sample width.

The boundary conditions are:

(i) No-slip at the microchannel walls

$$u_{sh}^*\big|_{\frac{y^*}{\alpha}=\frac{1}{2\alpha}}=u_{sh}^*\big|_{z^*=\frac{1}{2}}=u_s^*\big|_{z^*=\frac{1}{2}}=0. \tag{5}$$

(ii) Continuity of velocity and shear stress at the interface of the two fluids

$$u_s^*\big|_{\frac{y^*}{\alpha}=\frac{\omega}{2\alpha}}=u_{sh}^*\big|_{\frac{y^*}{\alpha}=\frac{\omega}{2\alpha}} \tag{6}$$

$$\left.\frac{\partial u_s^*}{\partial\left(\frac{y^*}{\alpha}\right)}\right|_{\frac{y^*}{\alpha}=\frac{\omega}{2\alpha}}=\frac{1}{\beta}\left.\frac{\partial u_{sh}^*}{\partial\left(\frac{y^*}{\alpha}\right)}\right|_{\frac{y^*}{\alpha}=\frac{\omega}{2\alpha}}. \tag{7}$$

(iii) Symmetry of the sample and sheath velocity profiles in y- and z-axes

$$\left.\frac{\partial u_s^*}{\partial z^*}\right|_{z^*=0}=\left.\frac{\partial u_{sh}^*}{\partial z^*}\right|_{z^*=0}=\left.\frac{\partial u_s^*}{\partial\left(\frac{y}{\alpha}\right)^*}\right|_{\frac{y^*}{\alpha}=0}=0. \tag{8}$$

Next, we apply the principle of mass conservation on both the fluids. The mass flow rate of the sample fluid through the inlet channel can be written in terms of the sample fluid density times the sample flow rate. It can further be expressed in terms of the average sample velocity. We obtain such a similar relationship for the sheath fluid as well. It is to be noted here that since we are considering fluids of different viscosities in our analysis, the average velocity for each fluid will have to be calculated separately over the region occupied by it in the cross-sectional plane. Thus, the sample fluid velocity is averaged between $(y^*/\alpha) = 0$ and $(y^*/\alpha) = (\omega/2\alpha)$ and the sheath fluid velocity is averaged between $(y^*/\alpha) = (\omega/2\alpha)$ and $(y^*/\alpha) = (1/2\alpha)$. Now, writing the expressions for the sample and sheath fluids, we obtain

$$\rho_s\frac{Q_s}{2}=\rho_s\overline{u_s}\frac{h}{2}\frac{w_f}{2} \tag{9}$$

where ρ_s is the sample fluid density, ρ_{sh} the sheath fluid density, Q_s the sample fluid flow rate, Q_{sh} the sheath fluid flow rate, $\overline{u_s}$ the area-average sample fluid velocity and $\overline{u_{sh}}$ is the area-average sheath fluid velocity.

$$\rho_{sh}\frac{Q_{sh}}{2}=\rho_{sh}\overline{u_{sh}}\frac{h}{2}\left(\frac{w_0-w_f}{2}\right). \tag{10}$$

Taking the ratio of the two equations above and using $\gamma = (\overline{u_s}/u_o)/(\overline{u_{sh}}/u_0) = \overline{u_s^*}/\overline{u_{sh}^*}$; where $\overline{u_s^*}$ is area-average normalized sample fluid velocity, $\overline{u_{sh}^*}$ the area-average normalized sheath fluid velocity, γ the ratio of average sample fluid velocity to average sheath fluid velocity, $\omega = w_f/w_0$ and $F = (Q_{sh}/Q_s)$ we obtain

$$\omega=\frac{1}{1+\gamma F}. \tag{11}$$

Here, F is a known parameter since Q_s and Q_{sh} can be fixed by two separate pumps; γ, however, is an unknown. To find γ, we need to find explicit expressions for the two velocity profiles and then calculate the area-average velocities. Towards this end, we first solve eqs (3) and (4) along with the boundary conditions (eqs (5) to (8)) and obtain

$$u_s^*=\frac{-P}{8}+\frac{Pz^{*2}}{2}+\sum_{n=\text{odd}}^{\infty}P_n\cosh n\pi\left(\frac{y^*}{\alpha}\right)\cos n\pi z^* \tag{12}$$

and

$$u_{sh}^*=\frac{-P\beta}{8}+\frac{P\beta z^{*2}}{2}+\sum_{n=\text{odd}}^{\infty}\left(L_n\cosh n\pi\left(\frac{y^*}{\alpha}\right)+M_n\sinh n\pi\left(\frac{y^*}{\alpha}\right)\right)\cos n\pi z^* \tag{13}$$

where

$$P=\frac{h^2}{u_0}\frac{1}{Ln_s}\frac{\partial p}{\partial x^*}. \tag{14}$$

$$L_n = \frac{\frac{4P\beta}{(n\pi)^3}\sin\frac{n\pi}{2}\left[(\beta-1)\sinh n\pi\left(\frac{\omega}{2\alpha}\right)\sinh n\pi\left(\frac{1}{2\alpha}\right)-A\right]}{\left[\begin{array}{l}(\beta-1)\cosh n\pi\left(\frac{\omega}{2\alpha}\right)\sinh n\pi\left(\frac{\omega}{2\alpha}\right)\sinh n\pi\left(\frac{1}{2\alpha}\right)\\ -\cosh n\pi\left(\frac{1}{2\alpha}\right)A\end{array}\right]} \tag{15}$$

$$A = \left(\beta\left\{\sinh n\pi\left(\frac{\omega}{2\alpha}\right)\right\}^2 - \left\{\cosh n\pi\left(\frac{\omega}{2\alpha}\right)\right\}^2\right) \tag{16}$$

$$M_n = \frac{\left[\begin{array}{l}\frac{4P\beta(\beta-1)}{(n\pi)^3}\sin\frac{n\pi}{2}\sinh n\pi\left(\frac{\omega}{2\alpha}\right)\\ -(\beta-1)L_n\cosh n\pi\left(\frac{\omega}{2\alpha}\right)\sinh n\pi\left(\frac{\omega}{2\alpha}\right)\end{array}\right]}{\left(\beta\left\{\sinh n\pi\left(\frac{\omega}{2\alpha}\right)\right\}^2 - \left\{\cosh n\pi\left(\frac{\omega}{2\alpha}\right)\right\}^2\right)} \tag{17}$$

$$P_n = \frac{L_n\sinh n\pi\left(\frac{\omega}{2\alpha}\right) + M_n\sinh n\pi\left(\frac{\omega}{2\alpha}\right)}{\beta\sinh n\pi\left(\frac{\omega}{2\alpha}\right)}. \tag{18}$$

The area-average normalized sample and sheath fluid velocities are then computed from

$$\overline{u_s^*} = \frac{\int_0^{1/2}\int_0^{\omega/2\alpha} u_s^*\,\mathrm{d}\left(\frac{y^*}{\alpha}\right)\mathrm{d}z^*}{\int_0^{1/2}\int_0^{\omega/2\alpha}\mathrm{d}\left(\frac{y^*}{\alpha}\right)\mathrm{d}z^*}. \tag{19}$$

$$\overline{u_{sh}^*} = \frac{\int_0^{1/2}\int_{\omega/2\alpha}^{1/2\alpha} u_{sh}^*\,\mathrm{d}\left(\frac{y^*}{\alpha}\right)\mathrm{d}z^*}{\int_0^{1/2}\int_{\omega/2\alpha}^{1/2\alpha}\mathrm{d}\left(\frac{y^*}{\alpha}\right)\mathrm{d}z^*}. \tag{20}$$

Putting the expressions from eqs (12) and (13) in (19) and (20) respectively, we obtain the following expression for γ

$$\gamma = \frac{\frac{-P}{48}\left(\frac{\omega}{\alpha}\right) + \sum_{n=\mathrm{odd}}^{\infty}\frac{1}{(n\pi)^2}\sin\left(\frac{n\pi}{2}\right)P_n\sinh n\pi\left(\frac{\omega}{2\alpha}\right)}{\frac{-P\beta}{24}\left(\frac{1-\omega}{2\alpha}\right) + \sum_{n=\mathrm{odd}}^{\infty}\frac{1}{(n\pi)^2}\sin\left(\frac{n\pi}{2}\right)B}\frac{1-\omega}{\omega}, \tag{21}$$

where

$$B = \left(\begin{array}{l}\left[L_n\sinh n\pi\left(\frac{1}{2\alpha}\right) - L_n\sinh n\pi\left(\frac{\omega}{2\alpha}\right)\right]\\ +\left[M_n\cosh n\pi\left(\frac{1}{2\alpha}\right) - M_n\cosh n\pi\left(\frac{\omega}{2\alpha}\right)\right]\end{array}\right). \tag{22}$$

Note that γ is a function of ω and vice versa. Thus, we have to employ an iterative procedure from which the width of the hydrodynamically focused sample fluid can be calculated (using eqs (11) and (21)). The expressions derived above can be used to calculate the hydro-dynamically focused width for any viscosity ratio, aspect ratio and flow ratio. Further, they can also be used to calculate other quantities such as the velocity and shear rate of both the fluids, either at a particular point or spatially averaged. This also allows us to study the variation of these quantities with the three basic parameters – flow ratio, aspect ratio and viscosity ratio, as discussed in detail here. A brief note explaining the use of the above equations is provided in Appendix B for convenience.

Discussion on the limiting cases

We provide an understanding of the variation of the focused sample width through its behaviour in the limiting cases. In the process, we answer the question of whether the sample width can be made zero. Apart from these limiting cases, the behaviour at intermediate values of the governing parameters are presented in the following section.

(I) *Variation with flow ratio (F)*

(i) $F \to 0$: As can be grasped intuitively, an extremely small flow ratio would effectively imply that only the sample fluid flows through the channel. If that is the case, it is apparent that its width would be as large as the width of the channel itself. This can also be seen from eq. (11); as $F \to 0$, we obtain $\omega = 1$, or $w_f = w_0$.

(ii) $F \to \infty$: Physically speaking, this is the opposite of the above case. A flow ratio tending to infinity effectively implies that only the sheath fluid flows through the channel. Thus, in this case, it is clear that the sample width obtained will tend to zero. From eq. (11) as $F \to \infty$, we obtain $\omega = 0$, or $w_f = 0$.

(II) *Variation with aspect ratio (α)*

(i) $\alpha \to 0$: The limiting value of $1/\gamma$ from eq. (21) as $\alpha \to 0$ is β. Thereafter, from eq. (11), we obtain

$$\omega = \frac{\beta}{\beta + F}. \tag{23}$$

(ii) $\alpha \to \infty$: Again, taking the limiting value of $1/\gamma$ from eq. (21) as $\alpha \to \infty$ and substituting it in eq. (11), we obtain the same result as in eq. (23).

Thus, we see that the expression for ω in both the limiting cases turns out to be the same. Therefore ω is a non-monotonic function of aspect ratio. The effect of variation in aspect ratio on ω is given special emphasis in the following section.

(III) *Variation with viscosity ratio (β)*

(i) $\beta \to 0$: This case could be physically thought of as the sample fluid being inviscid and the sheath fluid having some finite viscosity. From eq. (23), we obtain a value of $\omega = 0$ when $\beta \to 0$ for very low and very high aspect ratios (and any finite value of F). Thus, we see that a viscous sheath fluid compresses an inviscid sample fluid completely (in the limiting case). Physically, this happens because of the continuity of shear stress at the interface of the fluids (eq. (7)). As the RHS of eq. (7) tends to infinity, the velocity gradient of the sample should tend to infinity; which implies that the sample width ω should go to zero.

(ii) $\beta \to \infty$: This is opposite to the above case, as it could be thought of as the sheath fluid being inviscid and the sample fluid having some finite viscosity. Taking the limit of the RHS of eq. (23) using the expression for $1/\gamma$ from eq. (21), we obtain that $\omega = 1$, or $w_f = w_0$ (note that this is true for any finite flow ratio F). It is therefore difficult to compress a very viscous fluid using a sheath fluid having a much lower viscosity, irrespective of the flow ratio.

Comparison of theoretical expressions with literature

In this section, we show that the results available in the literature are special cases of the more general formula derived above.

Considering the case when $\alpha \ll 1$ and $\beta \neq 1$, the expression given in eq. (11) simplifies to the one in eq. (23). This agrees with the result given by Brown *et al.*[29]. Further, putting $\beta = 1$ in eq. (23), we obtain

$$\omega = \frac{1}{F+1}, \tag{24}$$

which is the result obtained by Stiles *et al.*[21].

Putting $F = 1$ in eq. (23) and writing $\beta = \eta_s/\eta_{sh}$, we obtain

$$\omega = \frac{\eta_s}{\eta_s + \eta_{sh}}, \tag{25}$$

which is the same as that given by Chang and Yang[30].

The expression for γ obtained by Lee *et al.*[11] is defined as the ratio of mean sample velocity and mean outlet velocity. This modified expression can be written as $\gamma^* = \overline{u_s^*}/(\overline{u_s^*} + \overline{u_{sh}^*})$ further putting $\beta = 1$ we obtain

$$\gamma^* = \frac{1 - \frac{192\alpha}{\omega\pi^5}\sum_{n=0}^{\infty}\frac{1}{(2n+1)^5}\frac{\sinh[(2n+1)\pi\omega/2\alpha]}{\cosh[(2n+1)\pi/2\alpha]}}{1 - \frac{192\alpha}{\pi^5}\sum_{n=0}^{\infty}\frac{\tanh[(2n+1)\pi/2\alpha]}{(2n+1)^5}}, \tag{26}$$

which again agrees with that given by Lee *et al.*[11]. Thus, eq. (11) encompasses the effects of all the parameters affecting the focused width and helps to calculate the hydrodynamically focused width by quantifying the magnitude of these factors.

Experimental setup and procedure

This section provides a description of the experimental setup, including design and fabrication of microchannels, and sample width detection principle employed in the experiments.

Fabrication of microchannel

The entire fabrication was done in-house[31–33]. A standard two-inch silicon wafer was used as the starting substrate. Conventional photolithography techniques were used to fabricate a cross-shaped microchannel; a schematic of the microchannel is shown in Figure 1 *d*. The width of all the arms of the microchannel was kept at 200 μm. SU8 photoresist (MicroChem Corp.) was spin coated on the wafer to obtain a depth of either 58 or 92 μm. This was followed by pre-baking, exposure to ultra-violet light and post-baking. The wafer was then developed to obtain the final SU8 mould structure. Once the mould is ready, a 10 : 1 mixture (w/w) of PDMS and curing agent was prepared and poured over the mould. The mould was then cured at 70°C for 1 h. Subsequently, PDMS was peeled off from the SU8 mold structure and holes were punched at the locations where the reservoirs were located. The PDMS chip was bonded to a glass slide, with a thin intermediate adhesive layer of PDMS[32]. Finally, the inlet and outlet tubes were attached to the reservoir holes.

A schematic of the experimental setup is shown in Figure 1 *e*. The experimental setup consists of two syringe pumps (Harvard Apparatus, USA) for introducing the sample fluid/sheath fluid, master flex tubing and connectors. Images and videos were captured using a MIPS Magnus CCD camera (4× magnification; 25 fps) attached to a microscope. Before starting the experiment, the PDMS device was thoroughly flushed with de-ionized water and recording was performed once steady conditions had been attained.

Focused sample width detection principle

The width of the hydrodynamically focused stream was calculated using image analysis (in Matlab R2009b). Pixel-intensity was plotted along a line perpendicular to the direction of the flow at a location downstream of the microchannel junction. After the removal of noise, image analysis yielded three peaks, as shown in Figure 1 *c*. The peaks on the left and right correspond to the walls of

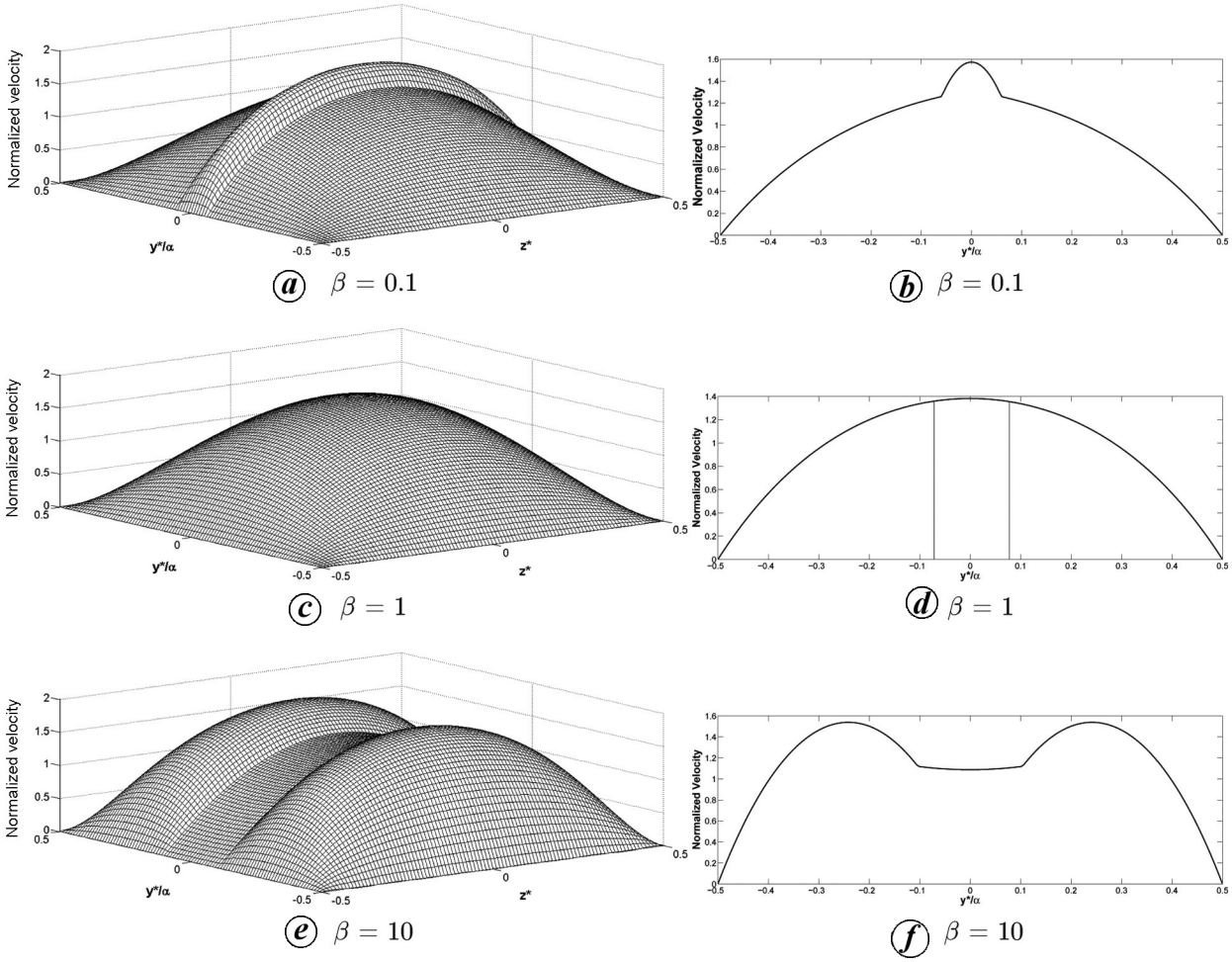

Figure 2. Effect of viscosity ratio on three-dimensional cross-sectional velocity profile for $\alpha = 1$ and $F = 4$. Corresponding two-dimensional graphs have been plotted at $z^* = 0.25$ in the right column.

the microchannel. The central peak corresponds to the sample stream. A Gaussian curve was fitted over this central peak (see Figure 1 *c*) and was used to calculate the width. Note that the sample width was resolved by at least eight points and widths were measures at a distance of 1 mm from the cross-junction (i.e. five times the microchannel width).

Theoretical results and discussion

The theoretical results are discussed along with a physical explanation of the results section. The results have been plotted over the range of parameters expected to be encountered in practical situations.

Effect of flow ratio and viscosity ratio

Equations (11) and (21) were solved as discussed in Appendix B to obtain the focused sample width. In Figure 2, the normalized cross-sectional velocity profile is plotted for viscosity ratios (i.e. β) of 0.1, 1 and 10. The velocity is normalized with respect to the overall average velocity in the outlet channel. As seen from Figure 2, for $\beta = 0.1$, the magnitude of the average sample fluid velocity is larger than that of the sheath fluid. Not only this, the average sample fluid velocity is also higher than the overall average velocity in the outlet channel. For $\beta = 1$, the situation is equivalent to that of a homogeneous fluid, and thus, the profile is similar to a paraboloid. For $\beta = 10$, the higher viscosity of the sample fluid leads to the average sample fluid velocity being lower than that of the sheath fluid. The relatively large sample width is apparent from the plot; the fluid spreads out laterally owing to its relatively low velocity. This observation is consistent with the requirement of equal shear stress at the interface of the two fluids (eq. (7)).

Figure 3 shows the normalized focused sample width plotted against the flow ratio for β values of 0.5, 1.0, 2.0, 5.0, 10 and 25 at two values of aspect ratio, $\alpha = 0.3$ and 10. As expected, the focused sample width decreases as F increases (Figure 3 *a*); this applies to all values of β.

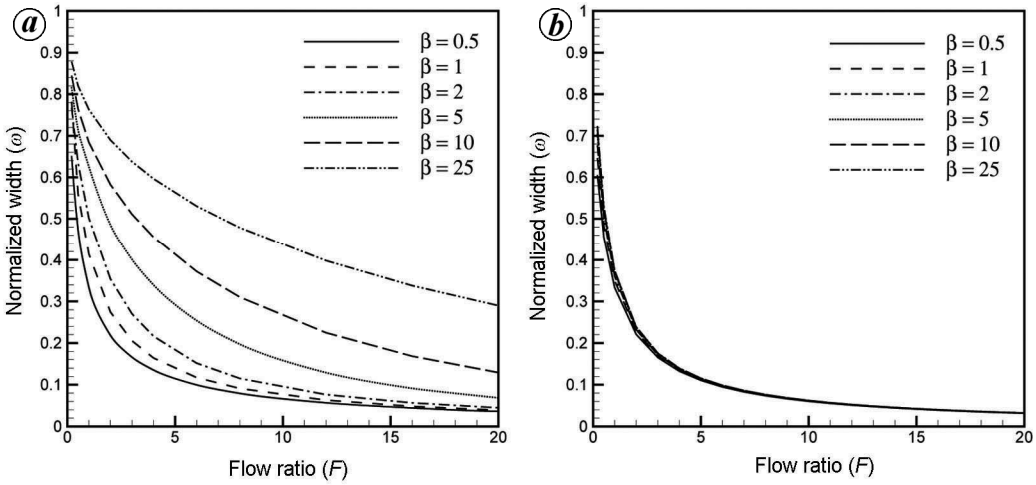

Figure 3. Effect of flow ratio on normalized width for different viscosity ratios at aspect ratio: ***a***, $\alpha = 0.3$; ***b***, $\alpha = 10$.

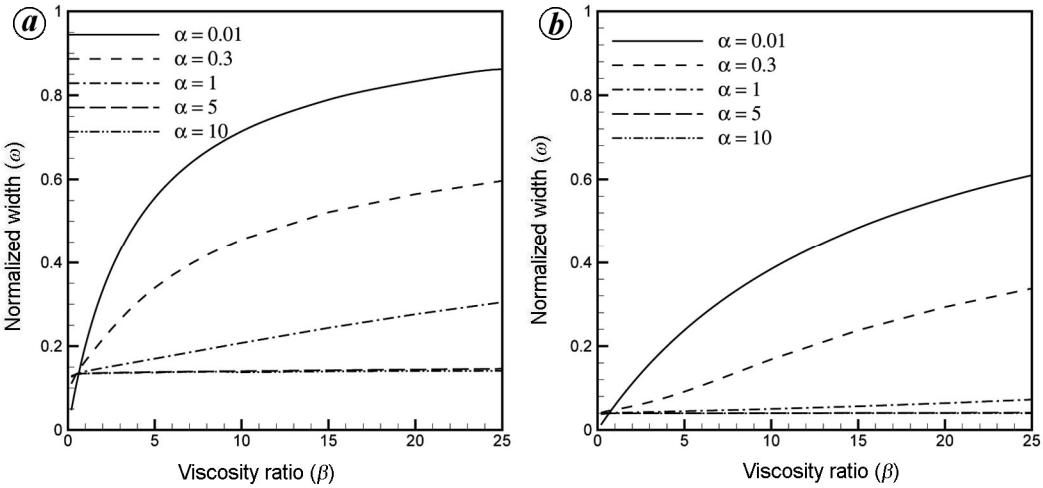

Figure 4. Effect of viscosity ratio on normalized width for different aspect ratios, at flow ratio: ***a***, $F = 4$; ***b***, $F = 16$.

Further, the focused sample width is higher at higher viscosity ratios, consistent with Figure 2. Figure 3 *b* however shows that the normalized width becomes independent of β values at high aspect ratio of 10 (as apparent from the merging of the curves). In fact, there is not much effect of viscosity ratio on the normalized width above aspect ratio of 2 for high flow ratios.

Figure 4 shows that as the viscosity ratio β increases, the focused sample width increases; this trend is followed for all values of F. For $F = 4$ and $F = 16$, the focused width is highest for $\alpha = 0.01$ and least when $\alpha = 10$ for cases when β is greater than a critical value (say β_{c1}; is critical value of viscosity ratio beyond which the normalized width decreases monotonically with increase in aspect ratio) and for cases where β is less than a critical value (say β_{c2}; is critical value of viscosity ratio below which the normalized width increases monotonically with increase in aspect ratio), this trend of focused width decreasing with increase in aspect ratio does not apply; this behaviour will be discussed further in the next section.

Effect of aspect ratio

To explore the effect of aspect ratio on the normalized width, we consider a range of β (0 to 25) and range of α (0.01 to 10). We find that when $\beta \geq 1$, the normalized width decreases with increase in aspect ratio for all values of F (Figure 5 *a*). For $\beta \leq 0.08$, the normalized width increases with increase in the aspect ratio, α for all values of F considered (Figure 5 *b*). For the intermediate values of β, the normalized width shows a non-monotonic trend. A physical explanation for this behaviour is offered in the following section.

The variation of normalized width with aspect ratio for β (0.05, 0.3, 0.5, 0.7 and 1) at $F = 0.2$ is shown in Figure 6 *a* and for same values of β at $F = 16$ in Figure 6 *b*. Notice from Figure 6 *a* that for $\beta = 0.05$, ω increases with increase in α; whereas for other values of β considered, ω decreases with increase in α. Similarly in Figure 6 *b*, ω increases with increase in α for $\beta = 0.05$ and decreases for $\beta = 1$, but for intermediate values of β, ω shows a

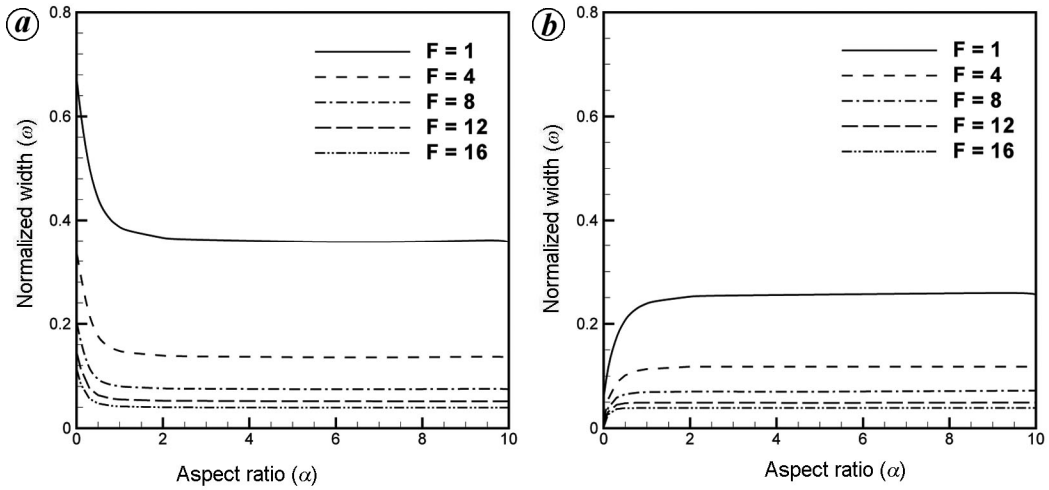

Figure 5. Effect of aspect ratio on normalized width for different flow ratios at viscosity ratio: ***a***, $\beta = 0.07$; ***b***, $\beta = 2$.

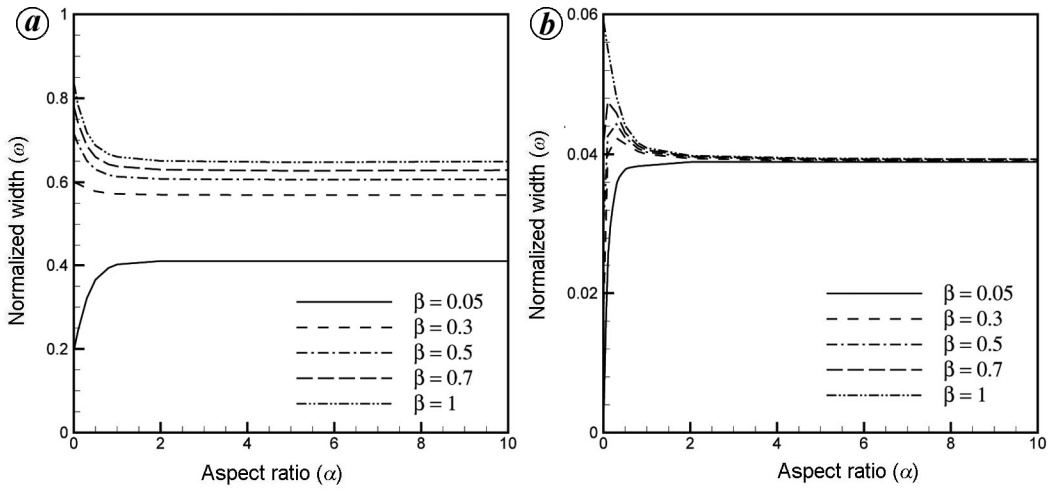

Figure 6. Effect of aspect ratio on normalized width for monotonic/non-monotonic range of viscosity ratio at flow ratio: ***a***, $F = 0.2$; ***b***, $F = 16$.

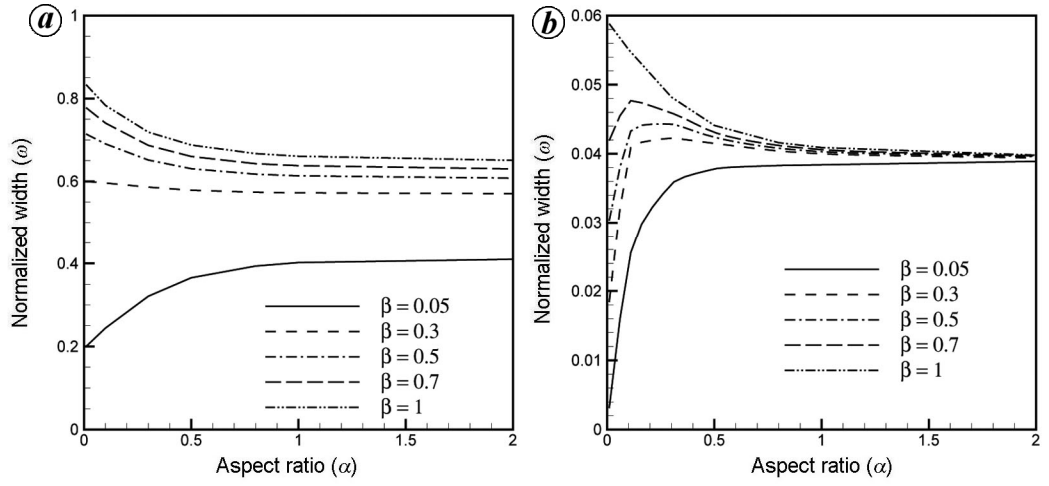

Figure 7. Exploded view of Figure 6 *a* and *b* for aspect ratio ranging from 0 to 2.

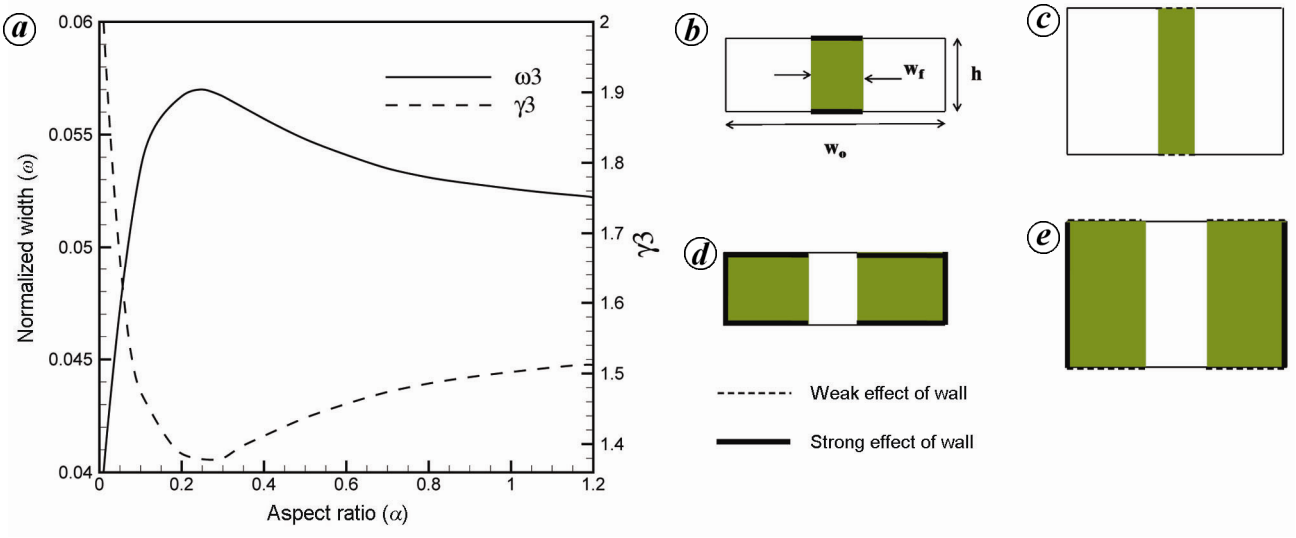

Figure 8. ***a***, Variation of normalized focused width ($\omega 3$) and ratio of average velocities ($\gamma 3$) versus aspect ratio for the case where $0.08 < \beta < 1$, $F = 12$, $\beta = 0.5$ (viscosity ratio is between β_{c2} and β_{c1}). (***b***–***e***) Schematic of variation in focused sample width with aspect ratio.

Table 1. Critical viscosity ratio range for monotonic nature of normalized width with variation in aspect ratios, for different range of flow ratios

	β_{c2}	β_{c1}
$0 < F \leq 1$	≤ 0.2	≥ 0.3
$1 < F \leq 8$	≤ 0.2	≥ 1
$8 < F \leq 12$	≤ 0.1	≥ 1
$12 < F \leq 16$	≤ 0.08	≥ 1

Table 2. Aspect ratios of microchannel providing minimum width of the sample under different condition of viscosity ratio and flow ratio

	$0 < F \leq 1$	$1 < F \leq 16$
$\beta \leq 0.2$	$\alpha \to 0$	
$0.2 < \beta < 0.7$	$\alpha \to 10$	$\alpha \to 0$
$\beta \geq 0.7$	$\alpha \to 10$	

non-monotonic trend. Figure 7 *a* and *b* represents exploded views of Figure 6 *a* and *b* respectively. Figure 6 *a* shows that the non-monotonic variation in the normalized width with aspect ratio is between β values of 0.05 and 0.3 and in Figure 6 *b*, it is between β values of 0.05 and 1. This suggests that there is a range of β values where the variation of ω with aspect ratio is non-monotonic and also flow ratio dependent.

Since in most cases of hydrodynamic focusing, a minimum sample focused width is desired, a relation pertaining to the effect of aspect ratio on the normalized width for known viscosity ratios will be useful in designing microchannels. Table 1 provides the values of viscosity ratios (β_{c1}, β_{c2}) above/below across which the variation of normalized width is monotonic with respect to variation in aspect ratio. Table 2 provides the value for aspect ratio of the microchannel to be considered to obtain the minimum sample focused width. Our analysis suggests that in order to attain minimum focused width, the designer should choose a high aspect ratio microchannel when $\beta \geq 1$ and a low aspect ratio microchannel is preferred when $\beta \leq 0.08$. However, when $0.08 \leq \beta \leq 1$, the normalized width varies non-monotonically with aspect ratio and is also dependent on the flow ratio; in such cases, one can refer to Table 2 and Figure 6 to obtain the minimum focused width of the sample. Tables 1 and 2 provide a ready reference for the optimal design of microchannels once the viscosity ratio of the fluids is known.

Reason for non-monotonicity in sample width with microchannel aspect ratio

An explanation for the trend in Figure 5 can be found by plotting γ (the ratio of the normalized average sample fluid velocity to the normalized average sheath fluid velocity, obtained from eq. (21)) and the normalized focused sample width (ω, obtained from eq. (11)) against the aspect ratio of the microchannel. Note that for a constant flow ratio, the normalized width and γ are inversely proportional. We consider three cases: $\beta \geq 1$; $\beta \leq 0.08$; and $0.08 < \beta < 1$ separately. In the first case, ω decreases and γ increases with the increase in aspect ratio. In the second case, ω increases and γ decreases with increase in aspect ratio of the microchannel. In Figure 8 *a* the variation of normalized width and γ values for the non-monotonic case ($0.08 < \beta < 1$) is shown. At $F = 12$ and $\beta = 0.5$, the normalized width first increases, then decreases with increase in the aspect ratio.

The next question is why the average sample fluid velocity exhibits such a behaviour as the aspect ratio is

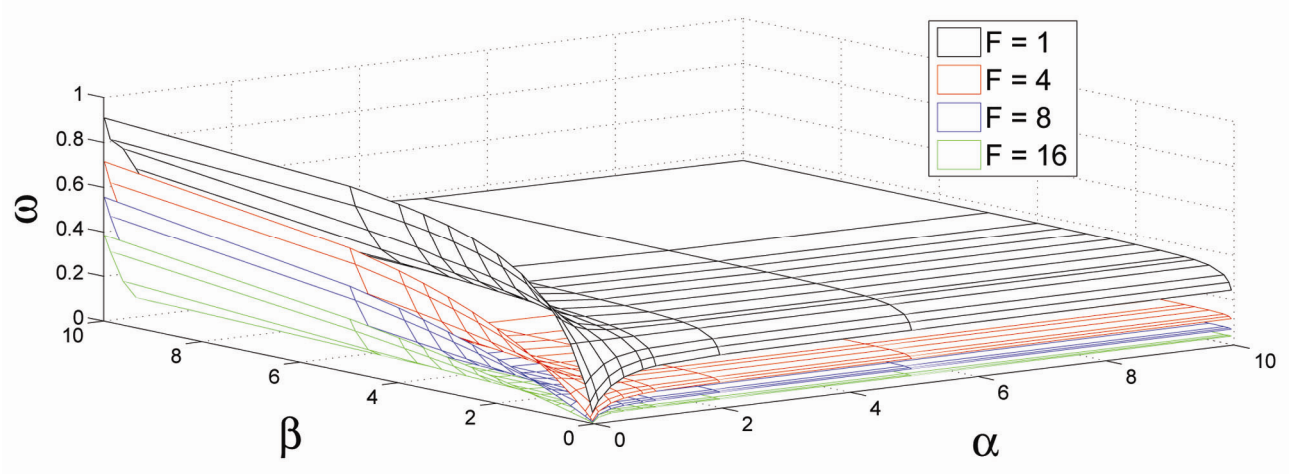

Figure 9. Normalized width, ω dependence on flow ratio F, viscosity ratio β and aspect ratio α.

increased. To address this, we consider the physical effects of increasing the aspect ratio, as depicted pictorially in Figure 8 *b* to *e*. For the case that the sample viscosity is higher than that of sheath ($\beta \geq 1$), as shown in Figure 8 *b*. The primary factor considered here are the no-slip conditions imposed by the upper and lower walls of the microchannel on the sample fluid, and the upper/lower as well as the side walls of the microchannel on the sheath fluid. At very low aspect ratios (Figure 8 *b*), the viscous effects due to the upper and lower walls of the microchannel on the sample fluid is relatively large (this is shown symbolically through thick lines at the upper and lower walls over the sample fluid) – this causes its average velocity to reduce. Since the flow rate is fixed, the sample fluid spreads over a larger width; thus, at very low aspect ratios, the focused sample width is high. Note here that because the aspect ratio is relatively small, the cross-section of the microchannel can be thought of as very wide (relative to the height) so that in this case, the effects of the side wall on the sheath fluid at the interface of the sheath and sample fluids is not significant. Now, keeping the width of the microchannel equal to that in Figure 8 *b*, we increase the height (and thus increase the aspect ratio), and arrive at Figure 8 *c*. Here, the upper and lower walls over the sample fluid are now farther apart than before and hence the viscous effects experienced by the sample fluid are also lesser in magnitude (this is shown by dashed lines at the upper and lower walls over the sample fluid). Here, the average sample fluid velocity increases and consequently, the focused sample width decreases (γ increases and ω decreases). Next, we consider the case when sample fluid viscosity is lesser (particularly $\beta < 0.08$) than the sheath fluid, shown in Figure 8 *d*. We increase the height of the microchannel and arrive at Figure 8 *e*. Here, the average velocity of the sample decreases (γ decreases and ω increases), leading to a higher focused sample width. Finally, we consider the situation when we choose the values of viscosity ratios and flow ratios in which the non-monotonic trend of normalized width was obtained, on plotting, we find that the normalized width, $\omega 3$ increases with increase in aspect ratio and then decreases with corresponding changes in $\gamma 3$.

Summary of the results

The theoretical results reveals that the normalized focused width depends on three major parameters, flow ratio, viscosity ratio of the fluids, and aspect ratio of the microchannel (Appendix A). An increase in the flow ratio results in a decrease in the normalized width of the sample fluid. An increase in the viscosity ratio of the fluid results in an increase in the normalized width of the sample fluid. However, with an increase in the aspect ratio of the microchannel, the normalized sample width may increase or decrease depending on the viscosity ratio of the fluids and the flow ratio employed. It is found that when $\beta \geq 1$, the normalized width of the sample decreases with increase in the aspect ratio of the microchannel for all values of flow ratios considered. When $\beta \leq 0.08$, the normalized width of the sample increases with increase in the aspect ratio of the microchannel for all values of flow ratios considered. However, when $0.08 \leq \beta \leq 1$, the normalized width of sample shows a non-monotonic trend with variation in the aspect ratio.

Figure 9 presents the combined effect of the governing parameters on the normalized width. The figure presents four surfaces at different flow rates. The topmost surface represents the variation of normalized width at flow ratio $F = 1$; in this case, the normalized width ω is relatively large. This is followed by surfaces at $F = 4$, 8 and 16 confirming that increasing flow ratio decreases the normalized width of the sample. Next, at a constant value of aspect ratio, α the normalized width increases with increase in the viscosity ratio, for all flow ratio values considered. At high values of aspect ratios and flow ratio,

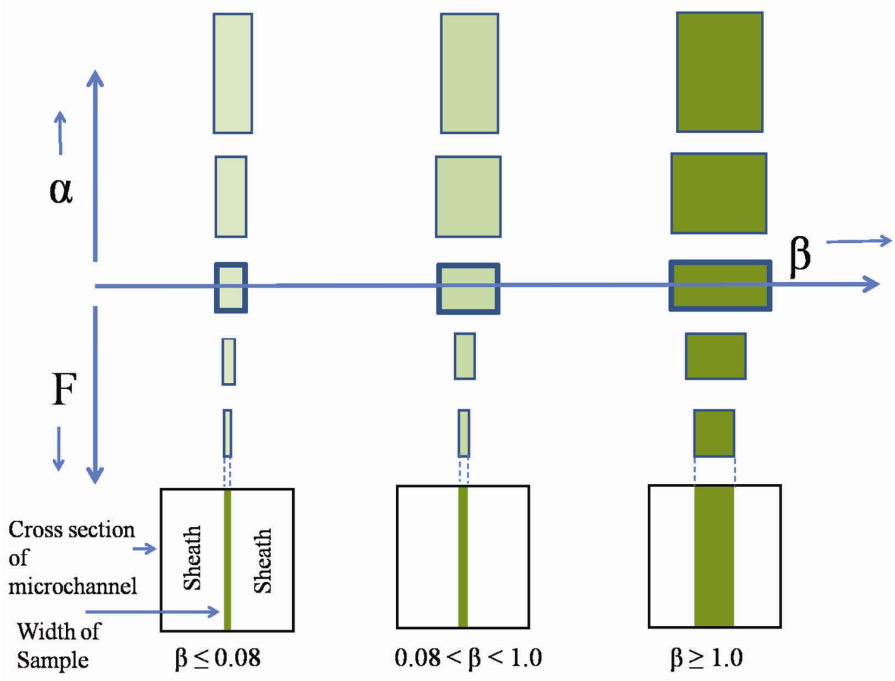

Figure 10. Qualitative depiction of the effect of the three governing parameters: flow ratio (F), viscosity ratio (β) and aspect ratio (α).

there is not much variation in the normalized width with respect to increase in the viscosity ratio. Further, on analysing the role of aspect ratio on normalized width, it can be observed from the figure that above $\beta = 1$, the normalized width decreases with increase in the aspect ratio and for $\beta \leq 0.08$, the normalized width increases with increase in the aspect ratio (notice folding of the curves).

Figure 10 is presented to provide a quick qualitative reference for visualizing the effects of the three parameters (flow ratio, viscosity ratio and aspect ratio) on the focused sample width. The rectangles shown correspond to the width of the sample stream. As shown, the focused sample width decreases rapidly as the flow ratio is increased – this is to signify that F has the strongest effect on the focused width. As the viscosity ratio (β) increases, the focused sample width also increases. The variation with aspect ratio (α) is shown through three cases: the left column describes the situation when $\beta \leq 0.08$ (the sample width increases asymptotically as aspect ratio is increased); the middle column corresponds to $0.08 < \beta < 1$ (the sample width increases and then decreases as the aspect ratio is increased), and the right column corresponds to $\beta \geq 1$ (the sample width decreases asymptotically as the aspect ratio is increased).

Comparison with experiments

Experiments were performed on the chips described earlier using oil and dyed water. The combination of dyed water (green in colour) and oil (transparent and colourless) was chosen to observe the effect of governing parameters on the normalized width. The oil viscosity was measured to be 0.0227 Pa-s and that of dye was 0.001 Pa-s at room temperature. Two separate sets of experiments were conducted: first, chip #1 having a depth of 58 μm ($\alpha = 0.3$) was used with oil as sample and then using oil as sheath. Next, chip #2 was used (depth 92 μm, $\alpha = 0.46$) and working fluids were utilized in the same manner as in chip #1. This enabled us to experimentally capture the effects of flow ratio, viscosity ratio and aspect ratio on the normalized width.

Figure 11 presents photographs (captured by a CCD connected to a microscope) showing the top-view of the microchannel depicting hydrodynamic focusing. Observe the effect of flow ratio on the normalized width from Figure 11 *a* and *b* where dyed water is used as the sample fluid. The normalized width decreases as the flow ratio is increased. A similar observation applies with oil as the sample fluid (Figure 11 *c* and *d*). We can observe the effects of viscosity on the normalized width by comparing Figure 11 *a* and *b* with Figure 11 *c* and *d* respectively. Notice that a higher flow ratio is required to compress a viscous fluid; this means that as the viscosity ratio increases, the normalized width also increases.

Figure 11 *e* to *h* is of special interest; these were captured to confirm the effects of aspect ratio on the normalized width. When the sample fluid is less viscous than the sheath fluid; also the situation where the sample fluid is more viscous than the sheath fluid. As discussed earlier, above a particular β value ($\beta \geq 1$), the normalized width decreases with increase in aspect ratio and below a

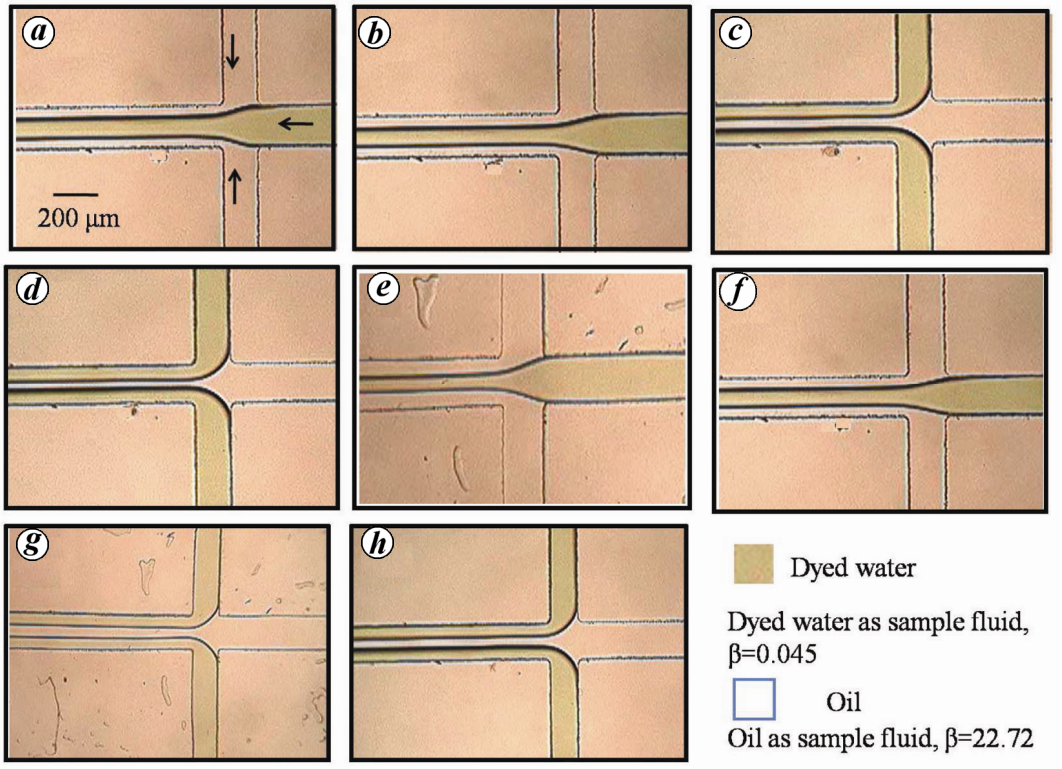

Figure 11. Photographs of experimental results with oil and dyed water for: ***a***, $F = 0.067$, $\alpha = 0.46$, $\beta = 0.045$; ***b***, $F = 0.2$, $\alpha = 0.46$, $\beta = 0.045$; ***c***, $F = 15$, $\alpha = 0.46$, $\beta = 22.72$; ***d***, $F = 20$, $\alpha = 0.46$, $\beta = 22.72$; ***e***, $F = 0.2$, $\alpha = 0.3$, $\beta = 0.045$; ***f***, $F = 0.2$, $\alpha = 0.46$, $\beta = 0.045$; ***g***, $F = 15$, $\alpha = 0.3$, $\beta = 22.72$; ***h***, $F = 15$, $\alpha = 0.46$, $\beta = 22.72$.

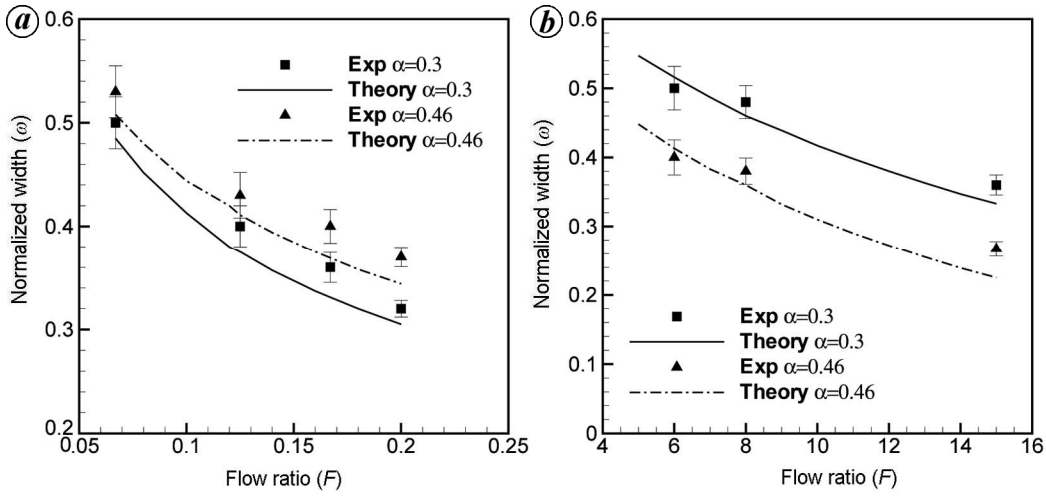

Figure 12. Comparison of theoretical predictions against experimental data for water–oil system with (***a***) dyed water as sample fluid and (***b***) oil as sample fluid.

particular β value ($\beta \leq 0.08$), the normalized width increases with increase in aspect ratio. It is observed in Figure 11 *e* and *f*, where $\beta = 0.045$, an increase in aspect ratio (0.3 to 0.46) leads to increase in normalized width, thus qualitatively confirming our theoretical analysis. Similarly, when $\beta = 22.72$, an increase in aspect ratio shows a decrease in normalized width (Figure 11 *g* and *h*). During the experiments, we kept the flow rate of oil as constant and varied the flow rate of dyed water. Upon lowering flow rates of dyed water below 80 μl/min, instability and plug flow were observed; and therefore data for those cases is not reported.

Figure 12 compares the experimental data quantitatively with the theoretical predictions. In Figure 12 *a*,

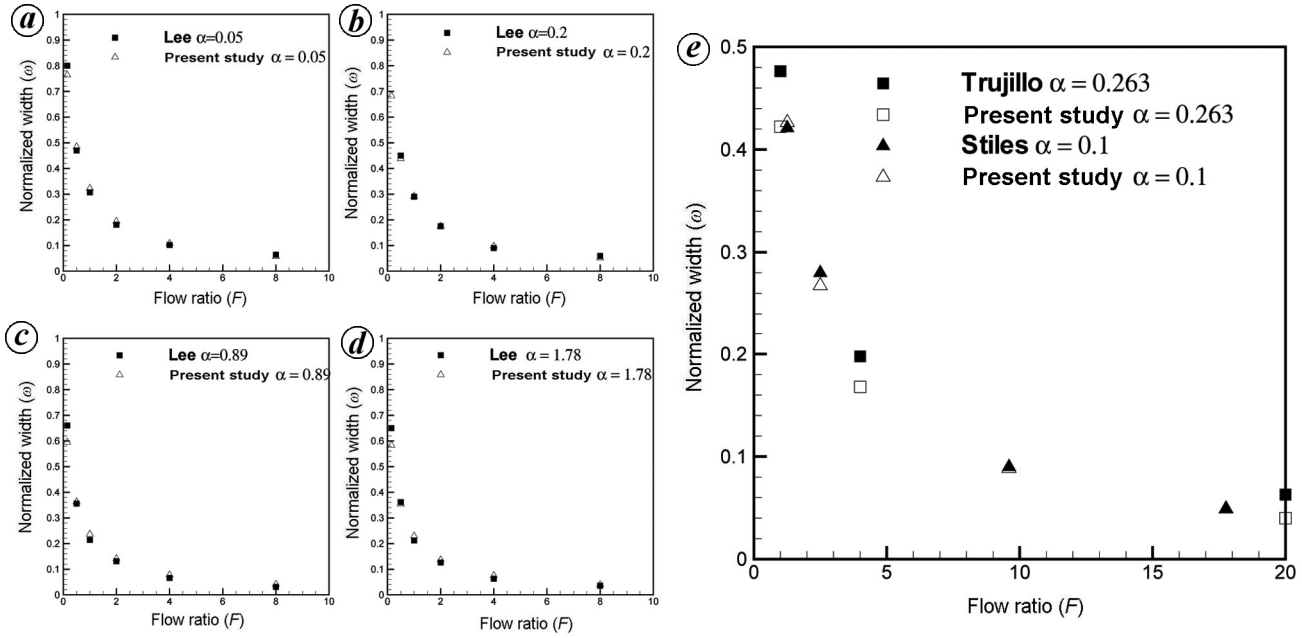

Figure 13. Comparison of our theory with Lee *et al.*[11]. Experimental data is provided for: ***a***, $\alpha = 0.05$; ***b***, $\alpha = 0.2$; ***c***, $\alpha = 0.89$; ***d***, $\alpha = 1.78$; at $\beta = 1$. ***e***, Comparison with Stiles *et al.*[21] and Trujillo *et al.*[22] for $\alpha = 0.263$ and 0.1 respectively.

dyed water is used as the sample fluid and in Figure 12 *b*, oil is used as the sample fluid. For all the cases investigated, the normalized focused width decreases as the flow ratio increases. The experimental data further affirms that the normalized width increases with increase in viscosity ratio. Flow ratios used for oil as sample fluid are much higher than the case when dyed water is used as the sample fluid. Furthermore, when viscosity ratio was 0.045, the normalized width was higher in higher aspect ratio microchannel ($\alpha = 0.46$) compared to the microchannel with lower aspect ratio ($\alpha = 0.3$). Similarly, when viscosity ratio was 22.72, the normalized width in microchannel ($\alpha = 0.46$) was lower compared to the microchannel with lower aspect ratio ($\alpha = 0.3$). Overall, the experimental data points compare well with the theory. However, some difference can be noted which may be because the sample fluid takes the form of a double concave along the height of the microchannel based on Reynolds number[19], but the relative comparison still remains valid.

Figure 13 *a* to *d* compares our theoretical results with those given by Lee *et al.*[11] at $\beta = 1$. We have also compared our results with Stiles *et al.*[21] and Trujillo *et al.*[22] in Figure 13 *e*. We note that our theoretical results are in good agreement with the experimental data (for all cases where experimental data is available). As mentioned briefly in the introduction, earlier researchers have developed formulae to calculate the focused sample width and studied its variation with one or more parameters. Stiles *et al.*[21] considered the sole effect of flow ratio. In this study, is shown that the combined effects of the flow ratio, aspect ratio and viscosity ratio can change the normalized width significantly. Based on the approach adopted by Brown *et al.*[29], for a flow ratio of 8 and viscosity ratio of 3, ω is 0.273. For the same parameters, our results show that if the aspect ratio is also taken into account, ω varies between 0.273 (at $\alpha = 0.01$) and 0.075 (at $\alpha = 10$), i.e. a variation of 75% can occur depending on the aspect ratio. Chang and Yang[30] have developed a theory which takes into account the combined effect of governing parameters on focused sample width, our theoretical results compares well with their theory.

Our theory is more general than the earlier studies, and the results in this section help to validate the theory, especially the monotonic and non-monotonic trends with aspect ratio and viscosity ratio.

Conclusions

The primary aim of this study was two-pronged: first, to develop theoretical expressions which can be easily employed to calculate the width of the focused sample stream. Second, to perform hydrodynamic focusing experiments and to evaluate the effect of governing parameters on the normalized focused width of the sample. The theoretical model showed that apart from the flow ratio (ratio of sheath fluid flow rate to sample fluid flow rate), the viscosity ratio (ratio of sample fluid viscosity to sheath fluid viscosity) and the aspect ratio (ratio of height of the microchannel to its width) also have a crucial role in determining the width of the focused sample stream.

The focused sample width decreases monotonically with an increase in the flow ratio and increases with increase in viscosity ratio of the fluids. An interesting

phenomenon emerged from the theoretical results which was validated experimentally – for viscosity ratios smaller than a critical value ($\beta_{c2} \leq 0.08$), the focused sample width increases as the aspect ratio of the microchannel is increased and for viscosity ratio greater than a critical value ($\beta_{c1} \geq 1$), the focused width decreases. However, there exists a range of viscosity ratio ($0.08 \leq \beta \leq 1$) in which the normalized width shows non-monotonic trend in normalized width with respect to variation in aspect ratio. Based on the results, one needs to know only the viscosities of the fluids involved and then refer to the design table to find the aspect ratio of the microchannel to be fabricated to obtain the minimum focused sample width. In the realistic range of aspect ratios (0.01 to 10) and flow ratios (0 to 16), for viscosity ratios of $\beta \geq 1$, one should choose a high aspect ratio channel, for $\beta \leq 0.08$, the choice should be a low aspect ratio channel to obtain a minimum focused width. However, if the β values lies in between the above range, one can refer to the design table for fabrication.

The presented model can be utilized in flow cytometry applications, controlling the interface between two parallel flowing liquids and in liquid/liquid microfluidic waveguides[29]. The results presented above are significant because they enable efficient and speedy design of microfluidic channels and reduce the number of iterations required to arrive at an optimized design for a desired amount of hydrodynamic focusing. This would, in turn, reduce design expenditure and human effort.

Appendix A: Dimensional analysis

This section shows that the theory developed in this study is indeed a complete model by showing that there are only three non-dimensional parameters that govern the magnitude of the focused sample width. The flow characteristics depend on three broad factors – the flow properties (flow rate of the fluids), fluid properties (density and viscosity of both the fluids), and geometric properties (height, width and length of the exit arm of the microchannel). We write this as follows

$$w_f = f(Q_s, Q_{sh}, \rho_s, \rho_{sh}, \eta_s, \eta_{sh}, h, w_0, L).$$

The theoretical model has been developed assuming fully developed flow. Thus, the flow profile does not depend on the location along the length of the channel, nor will there be any advective effects (which depend on density). Thus, we can eliminate the parameters L, ρ_s and ρ_{sh} from the above equation. The remaining parameters can be expressed in the following four non-dimensionalized groups: $\omega = w_f/w_0$, $F = Q_{sh}/Q_s$, $\beta = \eta_s/\eta_{sh}$ and $\alpha = h/w_0$. The above equation then reduces to

$$\omega = g(F, \beta, \alpha),$$

that is, for fully developed flow in microchannels, the non-dimensionalized focused sample width (ω) is completely described by the flow ratio (F), viscosity ratio (β) and aspect ratio of the microchannel (α).

Appendix B: Note on use of equations

This section outlines the procedure to theoretically calculate the focused sample width. Consider a microchannel with known geometric parameters (h and w_0) and sheath and sample fluids with known viscosities (η_{sh} and η_s, respectively). Let us assume that the flow rates of the sheath and sample fluid are Q_{sh} and Q_s respectively. From this, we calculate the ratios $\beta(\eta_{sh}/\eta_s)$, $\alpha(h/w_0)$ and $F(Q_{sh}/Q_s)$. Next, we need to solve for ω iteratively using eqs (11) and (21). For this, we need to use a procedure which updates the value of ω for each iteration, with the number of iterations being determined by the magnitude of error that is deemed to be acceptable for the purpose of the calculation (say 0.05%). Two variables need to be initialized for such a calculation – one to store the value of ω from the previous iteration, and the other to store the value of ω for the current iteration. Both these variables need to be initialized suitably. As soon as the error criterion is satisfied, the procedure (for instance, a 'while' loop) is exited and the value of ω at the end of these iterations is the final focused sample width.

1. Crosland-Taylor, P. J., A device for counting small particles suspended in fluid through a tube. *Nature*, 1953, **17**, 37–38.
2. Huh, D., Gu, W., Kamotani, Y., Grotberg, J. B. and Takayama, S., Microfluidics for flow cytometric analysis of cells and particles. *Physiol. Meas.*, 2005, **26**, R73–R98.
3. Lee, G. B., Lin, C. H. and Chang, S. C., Micromachine-based multi-channel flow cytometers for cell/particle counting and sorting. *J. Micromech. Microeng.*, 2005, **15**, 447–454.
4. de Mello, A. J. and Edel, J. B., Hydrodynamic focusing in microstructures, improved detection efficiencies in subfemtoliter probe volumes. *J. Appl. Phys.*, 2007, **101**, 084903.
5. Chung, S., Park, S. J., Kim, J. K., Chung, C., Han, D. C. and Chang, J. K., Plastic microchip flow cytometer based on 2- and 3-dimensional hydrodynamic flow focusing. *Microsyst. Tech.*, 2003, **9**, 525–533.
6. Lee, G. B., Hung, C. I., Ke, B. J., Huang, G. R., Hwei, B. H. and Lai, H. F., Hydrodynamic focusing for a micromachined flow cytometer. *J. Fluids Eng.*, 2001, **123**, 672–679.
7. Torisawa, Y. S., Mosadegh, B., Luker, G. D., Morell, M., O'Shea, K. S. and Takayama, S., Microfluidic hydrodynamic cellular patterning for systematic formation of co-culture spheroids. *Integr. Biol.*, 2009, **1**, 649–654.
8. Cosson, S., Allazetta, S. and Lutolf, M. P., Patterning of cell-instructive hydrogels by hydrodynamic flow focusing. *Lab. Chip*, 2013, **13**, 2099–2105.
9. Blankenstein, G. and Larsen, U. D., Modular concept of a laboratory on a chip for chemical and biochemical analysis. *Biosens. Bioelectron.*, 1998, **13**, 427–438.
10. Lee, G. B., Hung, C. I., Ke, B. J., Huang, G. R. and Hwei, B. H., Micromachined pre-focused $1 \times N$ flow switches for continuous sample injection. *J. Micromech. Microeng.*, 2001, **11**, 567–573.
11. Lee, G. B., Chang, C. C., Huan, S. B. and Yang, R. J., The hydrodynamic focusing effect inside rectangular microchannels. *J. Micromech. Microeng.*, 2006, **16**, 1024–1032.

12. Wong, P. K., Lee, Y. K. and Ho, C. M., Deformation of DNA molecules by hydrodynamic focusing. *J. Fluid Mech*., 2003, **497**, 55–65.
13. Knight, J. B., Vishwanath, A., Brody, J. P. and Austin, R. H., Hydrodynamic focusing on a silicon chip: mixing nanoliters in microseconds. *Phys. Rev. Lett*., 1998, **80**, 17.
14. Zhang, Z., Zhao, P., Xiao, G., Lin, M. and Cao, X., Focusing-enhanced mixing in microfluidic channels. *BioMicrofluidics*, 2008, **2**, 014101.
15. Park, H. Y. *et al.*, Achieving uniform mixing in a microfluidic device hydrodynamic focusing prior to mixing. *Anal. Chem*., 2006, **78**, 4465–4473.
16. Takeuchi, S., Garstecki, P., Weibel, D. B. and Whitesides, G. M., An axisymmetric flow-focusing microfluidic device. *Adv. Mater*., 2005, **17**, 1067–1072.
17. Moehlenbrock, M. J., Price, A. K. and Martin, R. S., Use of microchip-based hydrodynamic focusing to measure the deformation-induced release of ATP from erythrocytes. *Analyst*, 2006, **131**, 930–937.
18. Mielnik, M. M. and Saetran, L. R., Selective seeding for micro-PIV. *Exp. Fluids*, 2006, **41**, 155–159.
19. Blonski, S., Domagalski, P., Dziubinski, M. and Kowalewski, T. A., Selective seeding in micro-PIV. *Arch. Mech*., 2011, **63**(2), 163–182.
20. Kenis, P. J. A., Ismagilov, R. F., Takayama, S. and Whitesides, G. M., Fabrication inside microchannels using fluid flow. *Acc. Chem. Res*., 2000, **33**, 841–847.
21. Stiles, T., Fallon, R., Vestad, T., Oakey, J., Marr, D. W. M., Squier, J. and Jimenez, R., Hydrodynamic focusing for vacuum-pumped microfluidics. *Microfluid Nanofluid*, 2005, **1**, 280–283.
22. Trujillo, R. R., Mills, C. A., Samitier, A. J. and Gomila, G., Low cost micro-Coulter counter with hydrodynamic focusing. *Microfluid Nanofluid*, 2007, **3**, 171–176.
23. Stiles, P. J. and Fletcher, D. F., Hydrodynamic control of the interface between two liquids flowing through a horizontal or vertical microchannel. *Lab. Chip*, 2004, **4**, 121–124.
24. Wu, Z. and Nguyen, N. T., Hydrodynamic focusing in microchannels under consideration of diffusive dispersion: theories and experiments. *Sens. Actuators, B*, 2005, **107**, 965–974.
25. Galambos, P. and Forster, F., An optical micro-fluidic viscometer. In ASME International Mechanical Engineering Congress and Exposition, Anaheim, CA, 15–20 November 1998, pp. 187–191.
26. Olsen, C. K., Hoyland, J. D. and Rubahn, H. G., Influence of geometry on hydrodynamic focusing and long-range fluid behavior in PDMS microfluidic chips. *Microfluid Nanofluid*, 2012, **12**, 795–803.
27. Zhan, Y., Loufakis, D. N., Bao, N. and Lu, C., Characterizing osmotic lysis kinetics under microfluidic hydrodynamic focusing for erythrocyte fragility studies. *Lab Chip*, 2012, **12**, 5063–5068.
28. Chung, T. D. and Kim, H. C., Recent advances in miniaturized microfluidic flow cytometry for clinical use. *Electrophoresis*, 2007, **28**, 4511–4520.
29. Brown, M., Vestad, T., Oakey, J. and Marr, D. W. M., Optical waveguides via viscosity-mismatched microfluidic flows. *Appl. Phys. Lett.*, 2006, **88**, 134109.
30. Chang, C. C. and Yang, R. J., Hydrodynamic focusing effect on two-unmixed-fluid in microchannels. *Int. J. Nonlin. Sci. Num.*, 2008, **9**(3), 213–220.
31. Singh, S. G., Kulkarni, A., Duttagupta, S. P., Puranik, B. P. and Agrawal, A., Impact of aspect ratio on flow boiling of water in rectangular microchannels. *Exp. Therm. Fluid Sci*., 2008, **33**, 153–160.
32. Tripathi, S., Prabhakar, A., Kumar, N., Singh, S. G. and Agrawal, A., Blood plasma separation in elevated dimension T-shaped microchannel. *Biomed. Microdevices*, 2013, **15**(3), 415–425.
33. Prabhakar, A., Balavarun Kumar, Y. V., Tripathi, S. and Agrawal, A., A novel compact and efficient microchannel arrangement with multiple hydrodynamic effects for blood plasma separation. *Microfluid Nanofluid*, 2014; DOI: 10.1007/s10404-014-1488-6.

ACKNOWLEDGEMENTS. We acknowledge CEN, IIT Bombay (supported by the Department of Information Technology, MCIT, Government of India) for the fabrication facility.

Received 14 May 2014; revised accepted 6 August 2014